Evaluation of Modelling Methods for Electrocardiographic Fibrillatory Waves in Atrial Fibrillation

Jakub Grzelak[1], Shaheim Ogbomo-Harmitt[1], Fu Siong Ng[2], Andrew P King[1], Oleg Aslanidi[1]

[1]School of Biomedical Engineering and Imaging Sciences, King's College London, London, UK
[2]National Heart and Lung Institute, Imperial College London, London, UK

Abstract

The forward problem in electrocardiography maps epicardial activity to body surface potentials (BSPM), but the most detailed bidomain model with a finite element numerical solution is computationally expensive. We simulated sinus rhythm and atrial fibrillation activity in patient-specific 3D atria models (both volumetric and bilayer) and compared simplified infinite volume conductor method for forward BSMP calculation, against a ground truth pseudo-bidomain with finite element solution. Simplified models reproduced ECG morphology with high fidelity, while amplitudes were systematically underestimated due to absence of torso inhomogeneities. BSPM dynamics, including vector length and orientation, were well preserved, though gradients were exaggerated.

1. Introduction

The forward problem in electrocardiography defines the mathematical relationship between the heart's epicardial activations and the resulting body surface potential maps (BSPMs). One of its applications is the prediction of the standard 12-lead electrocardiogram (ECG) from known cardiac electrical sources, enabling mechanistic validation of clinical protocols and supporting the development of machine learning biomarkers [1]. A precise formulation of the forward problem is also essential for solving the inverse problem, which reconstructs cardiac electrical activity from BSPMs and provides a non-invasive alternative to intracardiac endocardial mapping used in clinics [2].

The bidomain model, solved using the finite element method (FEM), is widely regarded as the most biophysically detailed framework for calculating cardiac electrical activity and its projection to the body surface [3]. However, this approach is computationally demanding, requiring substantial processing time and memory, which limits its feasibility for large-scale in-silico studies or machine learning applications. To overcome these limitations, simplified methods with reduced computational complexity have been proposed, raising the question of how much anatomical and biophysical detail is truly necessary to achieve accurate forward simulations.

Although realistic heart and torso geometries are known to be important, the role of secondary structures such as lungs, fat, anisotropic skeletal muscle and other organs in shaping BSPMs remains debated [4]. While the Eikonal model with boundary element method has been shown to faithfully approximate bidomain [5], it was favoured in previous method comparisons largely because these relied primarily on correlation coefficients, which may be relatively insensitive measure that can underestimate the accuracy of other approaches [6]. Moreover, the Eikonal formulation cannot be used to simulate re-entry dynamics in AF, limiting its applicability. In a systematic validation study, Bear et al. compared in-vivo BSPMs with in-silico maps derived from epicardial recordings and reported substantial discrepancies when using a homogeneous infinite volume conductor torso model. Incorporating inhomogeneous torso conductivity reduced, but did not fully resolve, the differences [6].

In this study, we use patient-specific atrial anatomies to evaluate the accuracy of simplified forward models, specifically volumetric and bilayer monodomain 3D atrial models with infinite volume conductor torsos. The respective pseudo-bidomain model serves as the ground truth reference. We compare standard 12-lead ECGs and BSPMs for both P-waves in sinus rhythm (SR), which reflect atrial depolarization, and their pathological counterparts, the f-waves, seen in atrial fibrillation (AF).

2. Methods

2.1. Anatomical model

Patient-specific volumetric heart and torso models were derived from CT scans, complemented by high-resolution contrast-enhanced cardiac scans [7]. The model included the four-chamber heart, lungs, liver and blood pools with cardiac valves. Since the original patient

model was optimized for defibrillator and ventricular simulations, the atria lacked important details such as pulmonary veins, the left atrial appendage, and interatrial connections, all critical for realistic atrial propagation. To address this, we replaced the atria with electrophysiology-ready meshes [8] using Paraview [9] and Meshtool [10]. Utah IV atrial fibrosis maps [11] were projected onto both atria, preserving clinically observed spatial distribution and fibrotic tissue percentages [12]. A corresponding bilayer atrial model was generated using the atrialmtk pipeline [13, 14], and all atrial meshes were resampled to an average resolution of 340μm for simulations [15].

2.2. Electrophysiological modeling

Atrial myocyte electrophysiology was modelled using the Courtemanche et al. cell model [16], tuned to SR and AF ranges as described in our previous work [17]. Specifically, ionic channel conductivities were adjusted to reproduce regional heterogeneity and atrial action potential variability observed in AF. Conductivities were further optimized to match clinically reported conduction velocity ranges. Fibrosis remodelling included discrete fibrotic border zones, reduced conduction velocity, and electrophysiological remodelling related to cytokine and TGF-β1 signalling, as previously described [18].

2.3. Forward propagation methods

The bidomain model describes intra- and extracellular domains by coupled partial differential equations [3]. Since full bidomain simulations with FEM solvers were estimated to require ~188 days for this study, we adopted the pseudo-bidomain model as the ground truth (PB) [19]. This model introduces a thin augmentation layer around the tissue, replicating activation and bath-loading effects of the full bidomain. For comparison, we implemented monodomain propagation models, which reduce bidomain under the assumption of equal anisotropy ratios between intra- and extracellular conductivity tensors [20]. Forward BSPM calculations were performed with the infinite volume conductor method (IVC), assuming the heart is in a medium of uniform isotropic conductivity. Monodomain simulations were run on both volumetric (Vol-IVC) and bilayer (BL-IVC) atrial geometries.

2.4. Simulations

In-silico experiments were conducted with the PB, Vol-IVC and BL-IVC models in both SR and AF (re-entry) scenarios. For SR, excitation originated at the sinus node. AF was initiated by rapid pacing at the left superior pulmonary vein sleeve using an S1-S2 protocol with computed vulnerable window [21].

Simulations were performed with openCARP [22]. To ensure steady state, single cell pacing for 50 cycles was applied with basic cycle lengths of 500ms (SR) and 200ms (AF). A fixed timestep of 20μs was used. For BL-IVC volume-to-surface ratio was set to 1400cm^{-1} [14]. Simulation runtimes were: SR (1000ms): 25min (BL-IVC), 6h (Vol-IVC), 36h (PB); AF (2500ms): 1h (BL-IVC), 14h (Vol-IVC), 84h (PB). All runs were executed on a 16-core AMD Ryzen 9 7950X CPU.

2.5. Quantitative evaluation of models

Figure 1 presents simulated atrial activations and resulting BSPMs and for both SR and AF, along with the corresponding ECG leads II and V1. We evaluated the accuracy of simplified forward methods by comparing the Vol-IVC and BL-IVC to the ground truth PB. Performance was assessed using morphology metrics: Pearson Correlation; amplitude metrics: root mean squared potential (RMS), relative root mean squared error (rRMSE); and BSPMs characteristics at each time point: potential difference between extrema (ΔΦ), vector length (L) and orientation (θ) between extrema, and average potential attenuation adjacent to extrema (Amin/max) [6].

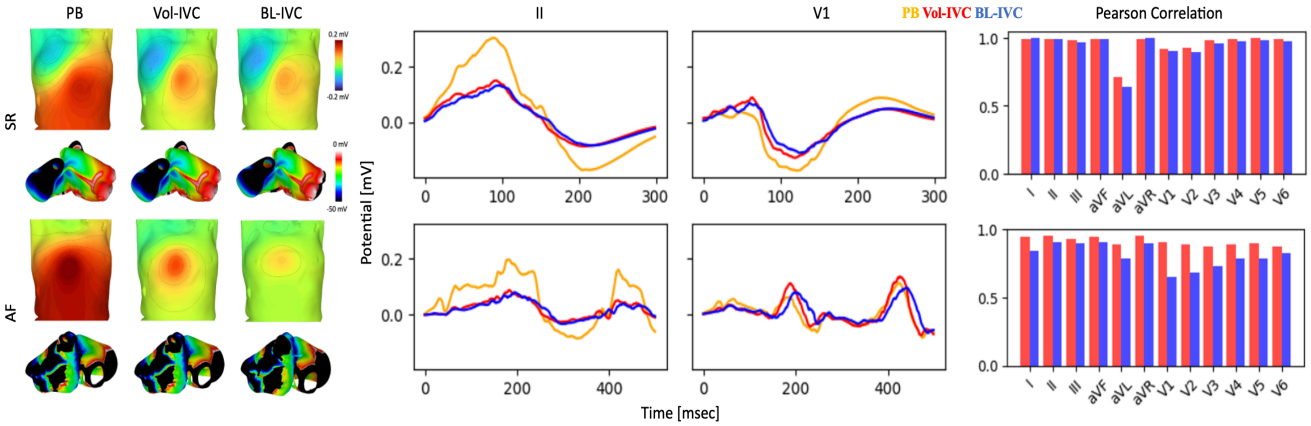

Figure 1. Simulation results: SR (top) and AF (bottom). Left: BSPMs and atrial activations. Middle: ECG leads II and V1 for PB (orange), Vol-IVC (red), BL-IVC (blue). Right: Pearson correlation of Vol-IVC and BL-IVC vs PB.

Metrics were analyzed at each time point over 300ms of the P-wave in SR and 500ms of the f-wave in AF [6] (Figure 2). Mean and standard deviations of the metrics for both SR and AF are presented in Tables 1 and 2.

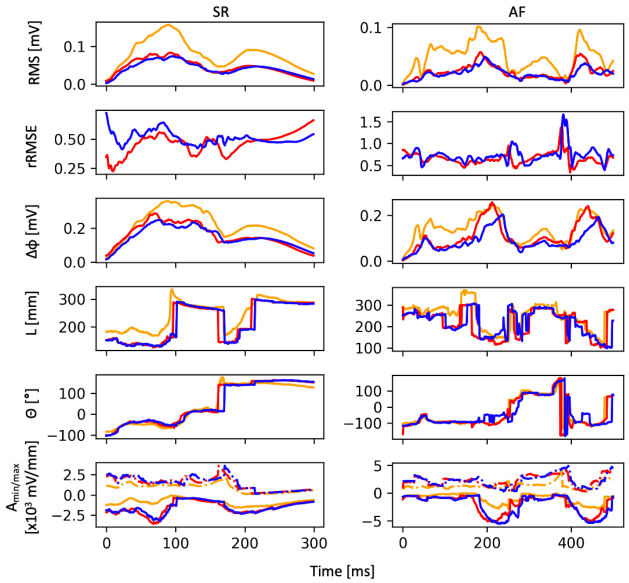

Figure 2. Evaluation metrics calculated at each time point of ECG for SR (left) and AF (right). PB (orange), Vol-IVC (red), BL-IVC (blue).

3. Results

3.1. Sinus rhythm

In SR, simplified models reproduced ECG morphology with high fidelity. Mean Pearson Correlation across the 12-lead ECG was 0.95±0.08 for Vol-IVC and 0.94±0.10 for BL-IVC, with values remaining >0.90 throughout the P-wave. Except, the lowest performance for aVL lead in both models, 0.71 and 0.63 respectively (Figure 1).

Amplitudes were systematically underestimated: PB RMS (0.08±0.04mV) was nearly double that of Vol-IVC (0.05±0.02mV) and BL-IVC (0.04±0.02mV). As shown in Figure 2, over the P-wave, RMS peaked early during atrial depolarization and then declined, with PB consistently maintaining higher amplitudes across the window. rRMSE remained relatively constant throughout cycle (0.46±0.08mV Vol-IVC; 0.51±0.05mV BL-IVC). BSPM characteristics followed expected temporal dynamics. Both ΔΦ and L peaked with maximal atrial activation and decreased as the P-wave terminated. PB consistently produced higher values than Vol-IVC and BL-IVC. However, PB length of the potential dipole was only 12% longer on average. Orientations remained stable and comparable. Attenuation near extrema was exaggerated in simplified models.

Table 1. Mean ± standard deviation of ECG and BSPM metrics (Pearson Corr, RMS [mV], rRMSE, ΔΦ [mV], L [mm], θ [°], $A_{min/max}$ [x10^3 mV mm^{-1}] computed across all time points of SR P-wave.

Metric	PB	Vol-IVC	BL-IVC
Corr	-	0.95±0.08	0.94±0.10
RMS	0.08±0.04	0.05±0.02	0.04±0.02
rRMSE	-	0.46±0.09	0.51±0.05
ΔΦ	0.22 ± 0.09	0.16±0.07	0.15±0.06
L	247±52	218±67	217±67
Θ	47.6±92.9	53.1±94.9	49.3±93.6
A_{min}	0.89±0.53	1.39±0.79	1.46±0.82
A_{max}	-0.89±0.38	-1.59±0.76	-1.56±0.73

3.2. Atrial fibrillation

During AF initiated from the left superior pulmonary vein, morphology accuracy decreased relative to SR, especially for the bilayer model. Vol-IVC maintained a mean correlation of 0.91±0.03, while BL-IVC dropped to 0.81±0.08. Temporal analysis revealed that correlation fluctuated with the complexity of wavefront dynamics: Vol-IVC maintained values near 0.9, while BL-IVC often dipped below 0.8 during periods of wave collision or fragmentation (Figure 1). These differences are linked to the bilayer model's mathematical formulation and atrial mesh structure, which produces slightly different dynamics compared to the volumetric approach [13, 14]. As a result, direct comparison is more difficult, and this is reflected in the somewhat lower correlations.

Amplitude discrepancies persisted in AF: PB RMS (0.05±0.02mV) was nearly double Vol-IVC and BL-IVC (0.02±0.01mV). RMS varied cyclically across the f-wave, reflecting reentrant dynamics, but PB consistently maintained higher amplitudes. rRMSE increased compared to SR (0.66±0.13mV Vol-IVC; 0.73±0.17mV BL-IVC), with greater variability during unstable propagation, see Figure 2.

Table 2. Mean ± standard deviation of ECG and BSPM metrics computed across all time points of AF f-wave.

Metric	PB	Vol-IVC	BL-IVC
Corr	-	0.91±0.03	0.81±0.08
RMS	0.05±0.02	0.02±0.01	0.02±0.01
rRMSE	-	0.66±0.14	0.73±0.17
ΔΦ	0.14±0.06	0.11±0.06	0.09±0.04
L	247±61	212±62	217±57
Θ	-40.9±83.6	-45.6±84.6	-41.3±81.1
A_{min}	1.31±0.58	2.21±0.97	2.16±1.09
A_{max}	-0.99±0.89	-2.04±1.58	-2.18±1.82

BSPM characteristics also displayed dynamic oscillations reflecting patterns linked to re-entry in AF. PB showed

larger ΔΦ (0.14±0.05mV) and 12% longer vector (246±60mm) than simplified models (~0.10mV and ~215mm), while orientations were similar. Attenuation remained consistently stronger in Vol-IVC and BL-IVC than in PB. We also investigated a scenario with AF initiated from the right superior pulmonary vein. While detailed results are not shown here, the outcomes were consistent with the left superior pulmonary vein case in both mean values and temporal dynamics.

4. Conclusions

Simplified models (Vol-IVC and BL-IVC) reproduced ECG morphology in SR and AF with high fidelity. A systematic underestimation of the ECG amplitudes can be due to the fact that the homogeneous IVC lacks the low-conductivity lungs included in the ground truth (PB). This primarily impacts RMS, rRMSE, and extrema-based ECG metrics, but such differences are mitigated in practice by normalization in clinical and machine learning workflows. Importantly, the overall ECG morphology and BSPM dynamics were accurately reproduced by the IVC approach at a fraction of the computational cost.

Acknowledgments

This work was supported by the EPSRC Digital Twins for Health CDT studentship (King's College London).

References

[1] M. A. Colman, O. V. Aslanidi, J. Stott, A. V. Holden, H. Zhang. "Correlation between P-wave morphology and origin of atrial focal tachycardia--insights from realistic models of the human atria and torso," IEEE Trans. Biomed. Eng., vol. 58, no. 10, pp. 2952-2955, Oct. 2011.

[2] A. J. Pullan, L. K. Cheng, M. P. Nash, C. P. Bradley, D. J. Paterson, "Noninvasive electrical imaging of the heart: theory and model development," Ann. Biomed. Eng., vol. 29, no. 10, pp. 817-836, Oct. 2001.

[3] L. Tung, "A bi-domain model for describing ischemic myocardial DC potentials", Ph.D. Dissertation, Massachusetts Inst. Technol., Cambridge, MA, USA, 1978.

[4] D. U. Keller, F. M. Weber, G. Seemann, O. Dössel, "Ranking the influence of tissue conductivities on forward-calculated ECGs," IEEE. Trans. Biomed. Eng., vol. 57, no. 7, pp. 1568-1576, Jul. 2010.

[5] C. Nagel, C. B. Espinosa, K. Gillette, et al., "Comparison of propagation models and forward calculation methods on cellular, tissue and organ scale atrial electrophysiology." IEEE Trans. Biomed. Eng., vol. 70, no. 2, pp. 511-522, Feb. 2023.

[6] L. R. Bear, L. K. Cheng, I. J. LeGrice, et al., "Forward problem of electrocardiography: is it solved?" Circ. Arrhythm., Electrophysiol., vol. 8, no. 3, pp. 677-684, Jun. 2015.

[7] S. Qian et al., "Additional coils mitigate elevated defibrillation threshold in right-sided implantable cardioverter defibrillator generator placement: a simulation study," Europace, vol. 25, no. 6, pp. euad146, Jun, 2023.

[8] C. Nagel, S. Schuler, O. Dössel, A. Loewe, "A bi-atrial statistical shape model for large-scale in silico studies of human atria: model development and application to ECG simulations," Med. Image. Anal., vol. 74, Dec. 2021.

[9] J. Ahrens et al., "ParaView: an end-user tool for large data visualization, handbook," Elsevier, 2005.

[10] A. Neic et al., "Automating image-based mesh generation and manipulation tasks in cardiac modeling workflows using meshtool," SoftwareX, vol. 11, 2020.

[11] C. H. Roney et al., "Predicting atrial fibrillation recurrence by combining population data and virtual cohorts of patient-specific left atrial models," Circ. Arrhythm. Electrophysiol., vol. 15, no. 2, Feb. 2022.

[12] N. Akoum et al., "Atrial fibrosis quantified using late gadolinium enhancement MRI is associated with sinus node dysfunction requiring pacemaker implant," J. Cardiovasc. Electrophysiol., vol. 23, no. 1, pp. 44-50, Jan. 2012.

[13] C.H. Roney et al., "Constructing bilayer and volumetric atrial models at scale," Interface Focus, vol. 13, Dec, 2023.

[14] S. Labarthe, J. Bayer, Y. Coudière et al., "A bilayer model of human atria: mathematical background, construction, and assessment," Europace, vol. 16, suppl. 4, pp. iv21-iv29, Nov. 2014.

[15] P. M. Boyle et al., "Characterizing the arrhythmogenic substrate in personalized models of atrial fibrillation: sensitivity to mesh resolution and pacing protocol in AF models," Europace, vol. 23, suppl. 1, pp. i3-i11, Mar. 2021.

[16] M. Courtemanche et al., "Ionic mechanisms underlying human atrial action potential properties: insights from a mathematical model," Am J Physiol, vol 275, no. 1, pp. H301–321, Jul, 1998.

[17] J. Grzelak et al., "In-silico investigation of the right and left atrial contributions to the P-wave morphology in ECG of healthy and atrial fibrillation patients," Computing in Cardiology (CinC), vol. 51, pp. 1-4, 2024.

[18] S. Ogbomo-Harmitt et al., "Effects of fibrotic border zone on drivers for atrial fibrillation: an in-silico mechanistic investigation," LNCS 2023, vol. 14507, pp. 174-185, Feb. 2024.

[19] M. J. Bishop and G. Plank, "Bidomain ECG simulations using an augmented monodomain model for the cardiac source," IEEE Trans Bio-Med Eng, vol. 58, no. 8, pp. 2297-2307, Aug, 2011.

[20] A. J. Pullan, M. L. Buist, L. K. Cheng, "Mathematically modelling the electrical activity of the heart: from cell to body surface and back again," World Scientific, 2005.

[21] M. Varela et al., "Atrial heterogeneity generates re-entrant substrate during atrial fibrillation and anti-arrhythmic drug action: mechanistic insights from canine atrial models," PLoS. Comput. Biol., vol. 12, no. 12, e1005245, Dec. 2016.

[22] G. Plank et al., "The openCARP simulation environment for cardiac electrophysiology," Comput Methods Programs Biomed, vol. 208, pp. 106223, Sep, 2021.

Address for correspondence:

Jakub Grzelak.
King's College London, Biomedical Engineering, Floor 3, Lambeth Wing, St Thomas' Hospital, London, SE1 7EH, UK.
jakub.grzelak@kcl.ac.uk